JOURNAL OF GEOPHYSICAL RESEARCH, VOL. 101, NO. B1, PAGES 571-583, JANUARY 10, 1996

Potbellies, wasp-waists, and superparamagnetism in magnetic hysteresis

L. Tauxe,[1] T.A.T Mullender, and T. Pick

Fort Hoofddijk Paleomagnetic Laboratory, Institute of Earth Sciences, University of Utrecht, Utrecht, Netherlands

Abstract. Because the response of a magnetic substance to an applied field depends strongly on the physical properties of the material, much can be learned by monitoring that response through what is known as a "magnetic hysteresis loop". The measurements are rapid and quickly becoming part of the standard set of tools supporting paleomagnetic research. Yet the interpretation of hysteresis loops is not simple. It has become apparent that although classic "single-domain", "pseudo-single-domain" and "multidomain" loops described in textbooks occur in natural samples, loops are frequently distorted, having constricted middles (wasp-waisted loops) or spreading middles and slouching shoulders (potbellies). Such complicated loops are often interpreted in oversimplified ways leading to erroneous conclusions. The physics of the problem have been understood for nearly half a century, yet numerical simulations appropriate to geological materials are almost unavailable. In this paper we discuss results of numerical simulations using the simplest of systems, the single-domain/superparamagnetic (SD/SP) system. Examination of the synthetic hysteresis loops leads to the following observations: (1) Wasp-waisting and potbellies can easily be generated from populations of SD and SP grains. (2) Wasp-waisting requires an SP contribution that saturates quickly resulting in a steep initial slope, and potbellies require low initial slopes (the SP contribution approaching saturation at higher fields). The approach to saturation is dependent on volume hence the cube of grain diameter. Therefore there is a very strong dependence of hysteresis loop shape on the assumed threshold size. (3) We were unable to generate potbellies using a SP/SD threshold size as large as 30 nm, and wasp waists cannot be generated using a threshold size as small as 8 nm. The occurrence of both potbellies and wasp waists in natural samples is consistent with a room temperature threshold size of some 15nm (+/- 5nm).(4)Simulations using a threshold size of 15-20 nm with populations dominated by SP grain sizes, that is with a small number of SD grains, produce synthetic hysteresis loops consistent with measured hysteresis loops and transmission electron microscopic observations from submarine basaltic glass. (5) Simulations and measurements using two populations with distinct coercivity spectra can also generate wasp-waisted loops. A relatively straightforward analysis of the resulting loops can distinguish the latter case from wasp-waisting resulting from SP/SD behavior.

Introduction

Highly sensitive magnetometers for measuring hysteresis properties of geological materials [e.g., *Flanders*, 1988] have recently become commonly available in paleomagnetic laboratories. So-called "hysteresis loops" are generated by subjecting a small sample to a very large magnetic field -Bmax- Such a magnetometer measures the magnetization of the sample as the applied field B decays to zero, approaches $-B_{max}$, then returns through zero to $+B$max- Many factors in the sample affect its response to the magnetic field, including but not limited to, mineralogy, particle size and shape, domain state, and particle interactions. If their individual contributions can be separated, a relatively quick procedure could yield a tremendous amount of information concerning these variables. The potential of rapid assessment of domain state, magnetic grain size, and/or magnetic mineralogy [e.g., *Wasilewski,* 1973; *Day et al,* 1977; *Parry,* 1980,1982; *Dunlop,* 1984,1986] has led many to incorporate hysteresis loop measurements into the routine battery of rock magnetic analyses accompanying paleomagnetic studies.

[1]Also at Scripps Institution of Oceanography, University of California, San Diego.

Paper number 95JB03041.
0148-0227/96/95JB-03041$05.00

However, the interpretation of hysteresis loops is not simple. Geological materials (and even many synthetic ones) are composed of particles with vastly different responses to magnetic fields and the resulting loops are distorted from the simple textbook examples suited for casual interpretation. While much progress has been made in determining the fundamental response of several geologically relevant minerals (magnetite [e.g., *Dayetal,* 1977; *Parry,* 1980,1982; *Heideretal,* 1987; *Worm andMarkert, l981;Hodych,* 1990; *Dunlop,* 1986; *Argyle and Dunlop,* 1990], pyrrhotite *[Dekkers,* 1988], goethite and hematite [e.g., *Hartstra,* 1982; *Dekkers,* 1988], and the hysteresis response of single crystals [e.g., *Enkin and Dunlop,* 1987; *Enkin and Williams*, 1994; *Williams and Dunlop,* 1989,1995] very little numerical modeling has been done to simulate hysteresis behavior resulting from mixtures of various minerals, grain sizes, or domain states (however see *Roberts et al,* [1995]). While *Sprowl* [1990] did investigate the effect of particle interaction in magnetite, most numerical modeling of hysteresis behavior has been done from an engineering point of view [e.g., *Jiles,* 1992; *Walker et al.*, 1993a, b; *Dellatorre et al,* 1994; *Basso et al,* 1994; *Friedman and May erg oyz,* 1992; *Ossart and Meunier,* 1991] and has not used geologically relevant parameters.

The importance of numerical modeling of hysteresis loops lies in the potential payoff: inverting hysteresis loops for the controlling grain size, domain state, and mineralogical components. Such inversions are theoretically possible, and similar types of inversions are carried out routinely in the medical and seismological communities. Before inversion is practical, however, a great deal more must be understood about the forward problem. The physical principles of the problem are well understood, but numerical simulation can be tricky and computationally intensive. In the following, we will show results from simulations of combinations of single-domain (SD) and superparamagnetic (SP) particles. These simulations model quite well the distorted hysteresis loops observed in many natural samples. As an additional benefit the combination of experimental and simulated data sets may provide constraints on the SP/SD threshold size.

Numerical Simulations of SP/SD Hysteresis Behavior: Uniaxial Anisotropy

Magnetic hysteresis loops from geological materials often differ from typical examples of single-domain (SD), pseudo-single-domain (PSD), and multidomain (MD) behavior. The loops can be distorted, making direct physical interpretation in terms of grain size or domain state difficult or impossible. The two most common types of distortion are (1) a constriction of the "waist" ("wasp-waisted") and (2) the less obvious but equally important "potbelly". Examples of representative loops derived from submarine basaltic glass (SBG) are shown in Figure la-c (see also examples in a variety of geological materials by e.g., *Jackson,* [1990], *Sun and Jackson,* [1994], *McCabe and Channell,* [1994], *Borradaile et aL,* [1993], *Channell and McCabe,* [1994], *Pick and Tauxe,* [1993, 1994], *Tarduno,* [1994], *Senanayake and McElhinny,* [1981], and *Roberts et aL,* [1995]). SBG has been shown by *Pick and Tauxe* [1994] to have a low-titanium magnetite as the magnetic phase. These loops can be categorized into four types: paramagnetic (not shown but is a straight line in these fields), single-domain (Figure la), potbellied (Figure lb), and wasp-waisted (Figure lc). Potbellied loops have not received attention in the literature, although we frequently see them in rock magnetic articles. Wasp-waisting, on the other hand, has been recognized for decades [e.g., *Wasilewski,* 1973] and can result from combining two magnetic phases with vastly different coercivities *[Wasilewski,* 1973] or combining superparamagnetic and single-domain behavior *[Pick and Tauxe,* 1993; *Jackson et aL,* 1993]. To investigate the effect of combining different hysteresis behaviors on the shape of the resulting loops, *Pick and Tauxe* [1994] modeled a linear combination of a population of SD grains with one of two SP populations of different initial slope. Figure Id shows the hysteresis loop for the SD population (dashed line) plus two approximate SP signals of different initial slope (solid lines). Figure le (solid line) displays the loop resulting from combining SD plus the shallow slope (SP1), and Figure If is SD plus the steeper slope (SP2). This simple model shows that the shape of the composite curve can indeed be dependent on the initial slope of the superparamagnetic population, but determining the actual distribution of magnetic grain sizes requires a more elaborate inverse modeling approach. In the following, we will use numerical simulation techniques to study combined superparamagnetic and uniaxial single domain behavior.

We will be investigating magnetic behavior as a function of an applied field. When the descending curve (the portion of the loop

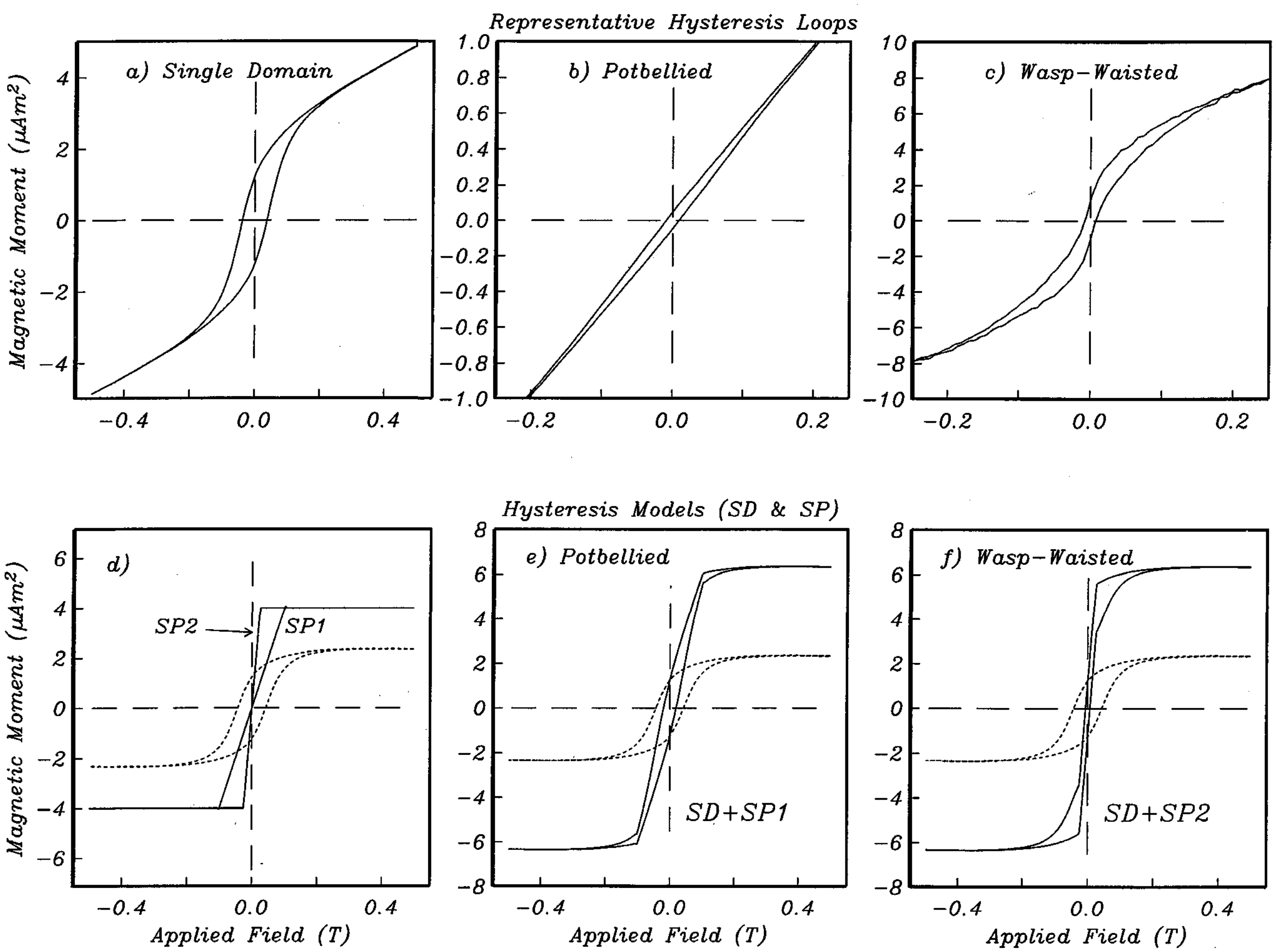

Figure 1. (a), (b), and (c) Characteristic hysteresis loops (uncorrected for paramagnetic slopes) for submarine basaltic glasses. (d), (e), aand (f) Qualitative models described in text.

traced between $B_{\max}$ and 0) and ascending curve (the portion traced between 0 and $B_{\max}$) are the same, there is no magnetic hysteresis; the treatment is reversible, and there is no magnetic remanence. Paramagnetic, diamagnetic, and superparamagnetic behavior are all reversible. We will ignore the strictly linear contributions in the following as these do not lead to the distortions illustrated in Figure 1. The superparamagnetic fraction, however, cannot be considered as a simple linear function in fields up to a Tesla (except for the very smallest particle sizes), and we begin by modeling the SP contribution to hysteresis loops.

Superparamagnetic Behavior

The starting point for our numerical simulations is an equation describing the magnetization M as a function of magnetic field B for a population of randomly oriented, noninteracting, single-domain particles, whose magnetization remains in thermal equilibrium with the applied field. Consider the particle with magnetic moment m drawn in Figure 2. SP particles, though small, are still single-domain and have one or more "easy" axes along which the energy is lower than the intervening "hard" axes. The so-called "anisotropy energy" (the energy required to change directions of magnetization from one easy direction to another) can result from several sources such as details of spin interactions (magnetocrystalline anisotropy), particle shape (magnetostatic anisotropy), and stress (magnetostrictive anisotropy). The simplest case to model is when there is just one preferred axis (uniaxial anisotropy), and we will start with this assumption for the numerical simulations presented here. The particle shown in Figure 2 has an easy axis at an angle ϕ away from the applied field B. Using polar coordinates in which α is the angle between B and m and β is the angle between m and the plane containing both B and the easy axis. Here, θ, the angle between m and the easy axis, is given by spherical trigonometry as

$$\cos\theta = \cos\alpha\cos\phi + \sin\alpha\sin\phi\cos\beta. \tag{1}$$

The magnetic energy E_m per unit volume of the magnetic particle shown in Figure 2 is governed by two competing sources [e.g., *Stoner and Wohlfarth*, 1948]: the anisotropy energy (here assumed uniaxial with anisotropy constant K_u) which encourages alignment of m with the easy axis and the magnetostatic energy equal to $m \cdot B$, acting to align m with B. Since $m = M_s v$, where M_s is saturation magnetization and v is volume, we calculate energy per unit volume

$$E_m = K_u \sin^2\theta - M_s B \cos(\alpha). \tag{2}$$

In SP grains, $E_m v$ is balanced with thermal energy kT (where k is Boltzman's constant and T is absolute temperature). Given N grains with known grain volume (here assumed for simplicity to be d^3, where d is the diameter and n is the number of grains with orientations within a given patch interval $d\alpha$, $d\beta$), the population within each patch will be proportional to the patch size ($d\beta d\alpha \sin\alpha$) and also to the Boltzmann factor $\exp(-E_m v/kT)$. Thus

$$n(\alpha,\beta)d\alpha d\beta \propto e^{(\frac{-E_m v}{kT})}\sin\alpha d\alpha d\beta. \tag{3}$$

The magnetization contributed to the "hysteresis" loop by grains within this interval is $M_s v n(\alpha,\beta)\cos\alpha$. And the total magnetization is

$$\frac{M}{M_s} = n_o \int_0^{\pi}\int_0^{2\pi} n(\alpha,\beta)d\beta\cos\alpha d\alpha, \tag{4}$$

where n_o is a proportionality factor taking into account the fact that integration over all $n(\alpha)d\alpha$ should equal N or

$$\int_0^{\pi} n(\alpha)d\alpha = N = 2\pi n_o \int_0^{\pi} e^{(M_s B v\cos\alpha)/kT}\sin\alpha d\alpha. \tag{5}$$

In the special case where the anisotropy energy is less than the thermal energy, it can be neglected eliminating the dependence on β. Following *Chikazumi and Charap* [1978], (3) then reduces to

$$n(\alpha)d\alpha = 2\pi n_o e^{(\frac{M_s B v \cos\alpha}{kT})}\sin\alpha d\alpha. \tag{6}$$

The total magnetization contributed by the N moments is now

$$\frac{M}{M_s} = \int_0^{\pi}\cos\alpha n(\alpha)d\alpha. \tag{7}$$

Combining (5) and (7) we get

$$\frac{M}{M_s} = N\frac{\int_0^{\pi} n(\alpha)\cos\alpha d\alpha}{\int_0^{\pi} n(\alpha)d\alpha}$$

$$= N\frac{\int_o^{\pi} e^{(M_s B v\cos\alpha)/kT}\cos\alpha\sin\alpha d\alpha}{\int_o^{\pi} e^{(M_s B v\cos\alpha)/kT}\sin\alpha d\alpha}.$$

By substituting $M_s Bv/kT = \gamma$ and $\cos\alpha = x$, we write

$$\frac{M}{M_s} = N\frac{\int_1^{-1} e^{\gamma x}x dx}{\int_1^{-1} e^{\gamma x}dx} = N\left(\frac{e^{\gamma}+e^{-\gamma}}{e^{\gamma}-e^{-\gamma}} - \frac{1}{\gamma}\right) \tag{8}$$

and finally

$$\frac{M}{M_s} = N(\coth\gamma - \frac{1}{\gamma}). \tag{9}$$

Our end result, (9), is called the "Langevin" function and also describes the magnetization of a paramagnetic gas; hence the term "superparamagnetic" for such particles [e.g., *Stacey and Banerjee*, 1974].

The contribution of SP particles for which the Langevin function is valid with given M_s and d is shown in Figure 3a. The field at which the population reaches 90% saturation B_{90} occurs at $\gamma \sim 10$. Assuming particles of magnetite (M_s = 4.5 x 10^5 A/m) and room temperature (T = 300°K), B_{90} can be evaluated as a function of d (see Figure 3b). The maximum size for SP behavior is generally taken to be ~ 30 nm [*Dunlop*, 1973], at which B_{90} is a few milliTesla. Because of its inverse cubic dependence on d, B_{90} rises

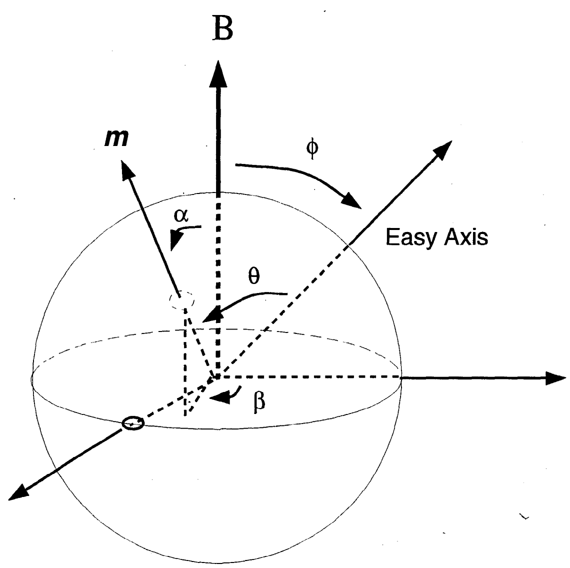

Figure 2. Sketch of particle with easy axis making an angle ϕ with the applied magnetic field B. The moment m has polar coordinates of α and β.

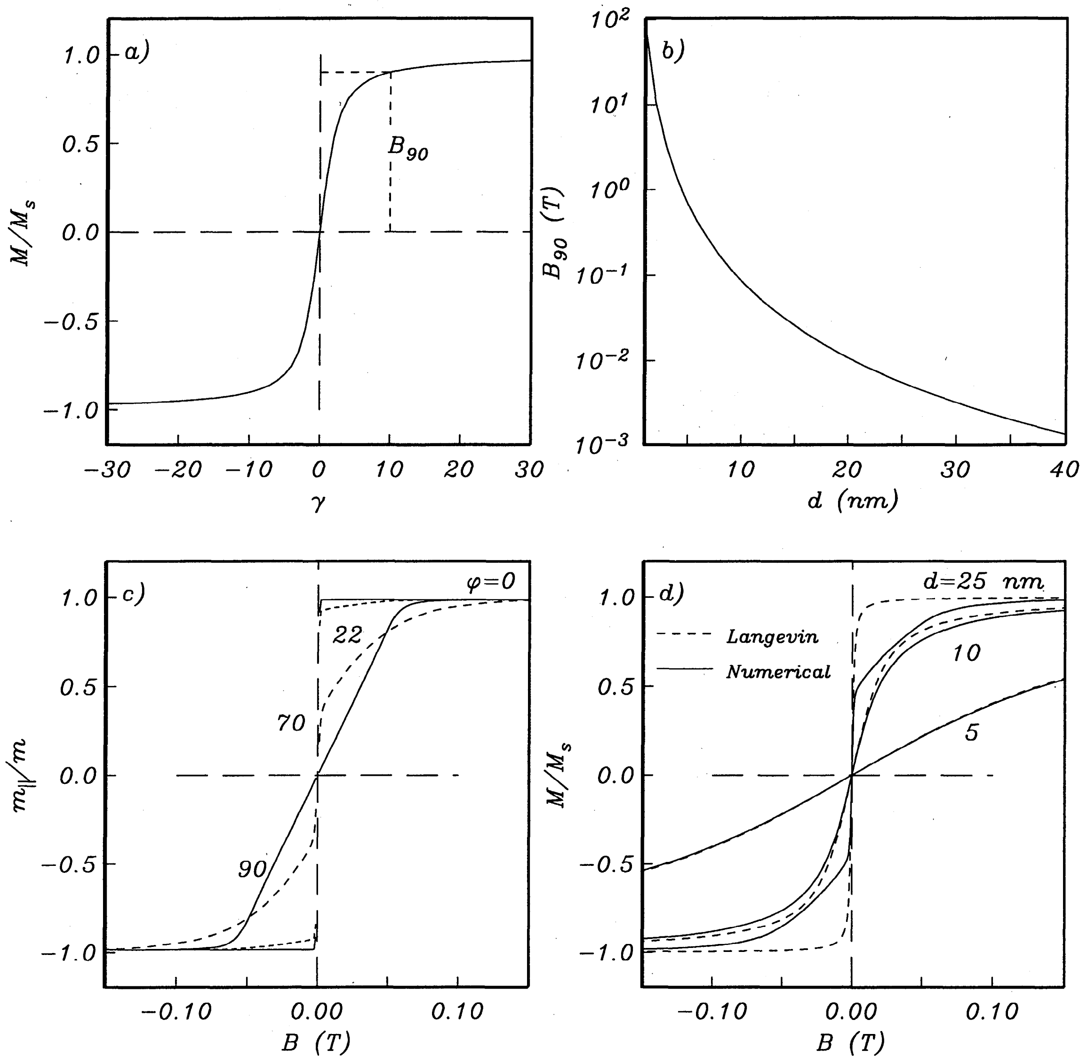

Figure 3. (a) The contribution of a population of SP particles with saturation magnetization M_s and cubic edge length d. Here, $\alpha = BM_s v/kT$. There is no hysteresis as both the ascending and descending loops are identical. The field at which the magnetization reaches 90% of saturation (B_{90}) is reached when $M_s d^3/kT \simeq 10$. (b) B_{90} as a function of d using appropriate values for magnetite at room temperature is shown (see text). (c) The SP contribution to hysteresis loops for grains with d = 25 nm and several values of ϕ done by numerical integration are shown. d) The contribution of an assembly of randomly oriented grains with various values of d to the hysteresis loop (solid lines) is shown. The Langevin solution for the same d values (dashed lines) is also shown.

sharply with decreasing d and is hundreds of Tesla for particles a few nanometers in size, approaching paramagnetic values.

For our first approximations we have neglected anisotropy energy in the SP grain sizes. In fact, for SP grains near the SD threshold size there may be significant anisotropy energy, and the resulting curves will be somewhat "flatter" than those predicted by purely Langevin behavior. Numerical integration of (3) for a given value of d = 25 nm and various values of ϕ give the curves shown in Figure 3c.

We generate synthetic "hysteresis" loops for a large population of particles of a given d, with easy axes uniformly distributed in space in the following manner. First, we draw values for ϕ from a uniform spherical distribution using the method outlined by *Fisher et al.* [1987]. That is, three random numbers (R_1, R_2, R_3) are drawn from a Gaussian distribution. (We use the subroutine GASDEV from *Press et al.* [1986] to generate Gaussian distributions.) Orientation of the easy axes are then given by

$$\phi = \cos^{-1}\frac{R_3}{\sqrt{R_1^2+R_2^2+R_3^2}} \tag{10}$$

We perform the numerical integration of (3) shown in Figure 1 and sum the contributions of many randomly oriented grains. Synthetic curves for three grain sizes are shown in Figure 3d. Also shown is the Langevin solution for the particular grain size. The numerical and Langevin curves superpose for grains as small as 5 nm. Since anisotropy energy is equal to thermal energy for grains of about 7 nm, this should come as no surprise. For grains much larger than about 8 nm we see a deviation from the Langevin function (see curves for 10 and 25 nm), with the inclusion of anisotropy energy acting to slow the approach to saturation. The initial slopes, however, are similar. In our simulations we use the Langevin approximation for grains smaller than 8 nm and the numerical integration for grains between 8 and the SP/SD threshold. At this threshold we assume that the grains are no longer in thermal equilibrium with the field and that thermal energy is unimportant. We now describe our treatment of SD grains.

Single-Domain Behavior

The modeling of stable single-domain (SD) behavior is similar to our treatment of larger SP particles [see *Stoner and Wohlfarth*, 1948; *Friedman and Mayergoyz*, 1992; *Walker et al.*, 1993a, b]. The essential mathematics describing the energy of a particle with uniaxial anisotropy in the presence of a magnetic field was worked out by *Stoner and Wohlfarth* [1948] (see also *O'Reilly* [1984]). Consider a particle with uniaxial anisotropy whose easy axis makes an angle ϕ with the magnetic field B (see Figure 2). The magnetic moment m is drawn away from the easy axis, making an angle θ with the easy axis. Because thermal energy is insignificant, m is constrained to lie within the plane containing B and the easy axis ($\beta = 0$). The component parallel to $+B$ (which contributes to the net magnetization of the hysteresis loop) is given by $m_{||} = m$ cos(α), where $\alpha = \phi - \theta$. The energy of this particle is given by (2).

In the following, we are interested in the θ which corresponds to an energy minimum, as well as the B sufficient to cause a reversal in magnetization along the easy axis. Thus we need to determine the θ for which $dE/d\theta = 0$ and the B at which both $dE/d\theta = 0$ and $d^2E/d\theta^2 = 0$. The relevant equations are

$$\frac{dE}{d\theta} = 2K_u \sin\theta\cos\theta - M_s B \sin(\alpha) \qquad (11)$$

and

$$\frac{d^2E}{d\theta^2} = 2K_u \cos(2\theta) + M_s B \cos(\alpha). \qquad (12)$$

Setting K_u to 1.4 x 10^4 Jm^{-3} and normalizing by the saturation magnetization of magnetite (4.5 x 10^5 Am^{-1}, we calculate the variation of E and its first and second derivatives (expressed per unit magnetic moment) as a function of θ.

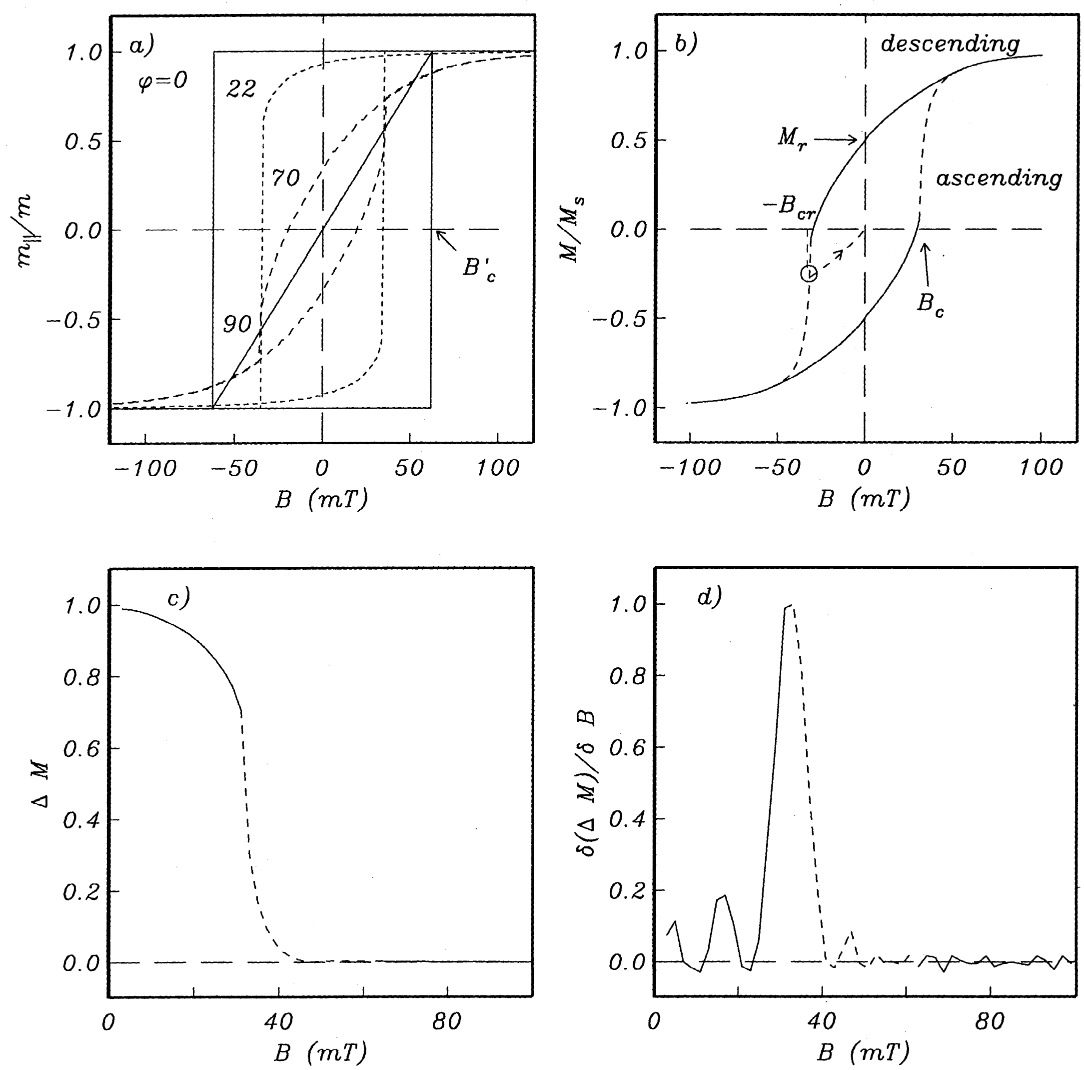

Figure 4. (a) The component of m parallel ($m_{||}$) to $+B_{\max}$ for various values of ϕ. The intrinsic coercive field is marked by B'_c. b) Sum of 10,000 individual curves similar to those shown in Figure 4a, for ϕ drawn from a uniform distribution on a sphere is shown. The saturation remanence M_r, bulk coercivity B_c, and coercivity of remanence B_{cr} are indicated. The reversible portions of loops are drawn as solid lines and the irreversible portions are dashed. (c) The ΔM curve of the data shown in Figure 4b is indicated. (d) The derivative of the curve shown in Figure 4c is indicated (see text).

When the easy axis is aligned parallel to the field (ϕ = 0), the moment remains undisturbed (with θ = 0) and the component of m parallel to B $m_{||}$ equals m (square loop in Figure 4a). The moment remains unchanged until the field, increasing along $-B$, is sufficiently large to cause the moment to flip suddenly; the contribution to the hysteresis loop ($m_{||}$) is now -m. This "flipping field" (B_f) can be evaluated as the field for which both $dE/d\theta$ and $d^2E/d\theta^2$ are zero. By solving (11) and (12) for B and using some trigonometric trickery, we get

$$B_f = \frac{2K_u}{M_s}(1 - \omega^2 + \omega^4)^{\frac{1}{2}}/(1 + \omega^2), \qquad (13)$$

where $\omega = tan\phi^{\frac{1}{3}}$. For ϕ = 0 (ω = 0), we define the flipping field to be the intrinsic coercivity B_c'. Returning to Figure 4 and following the ϕ = 0 curve from $-B_c'$ to $-B_{\max}$ and then to $B = 0$, there is no change in $m_{||}$ through -$B_{\max}$, back to zero. On its final approach to $+B_{\max}$ the moment will again flip at $+B_c'$ and $m_{||}/m$ = 1, or $m_{||} = M_s v$.

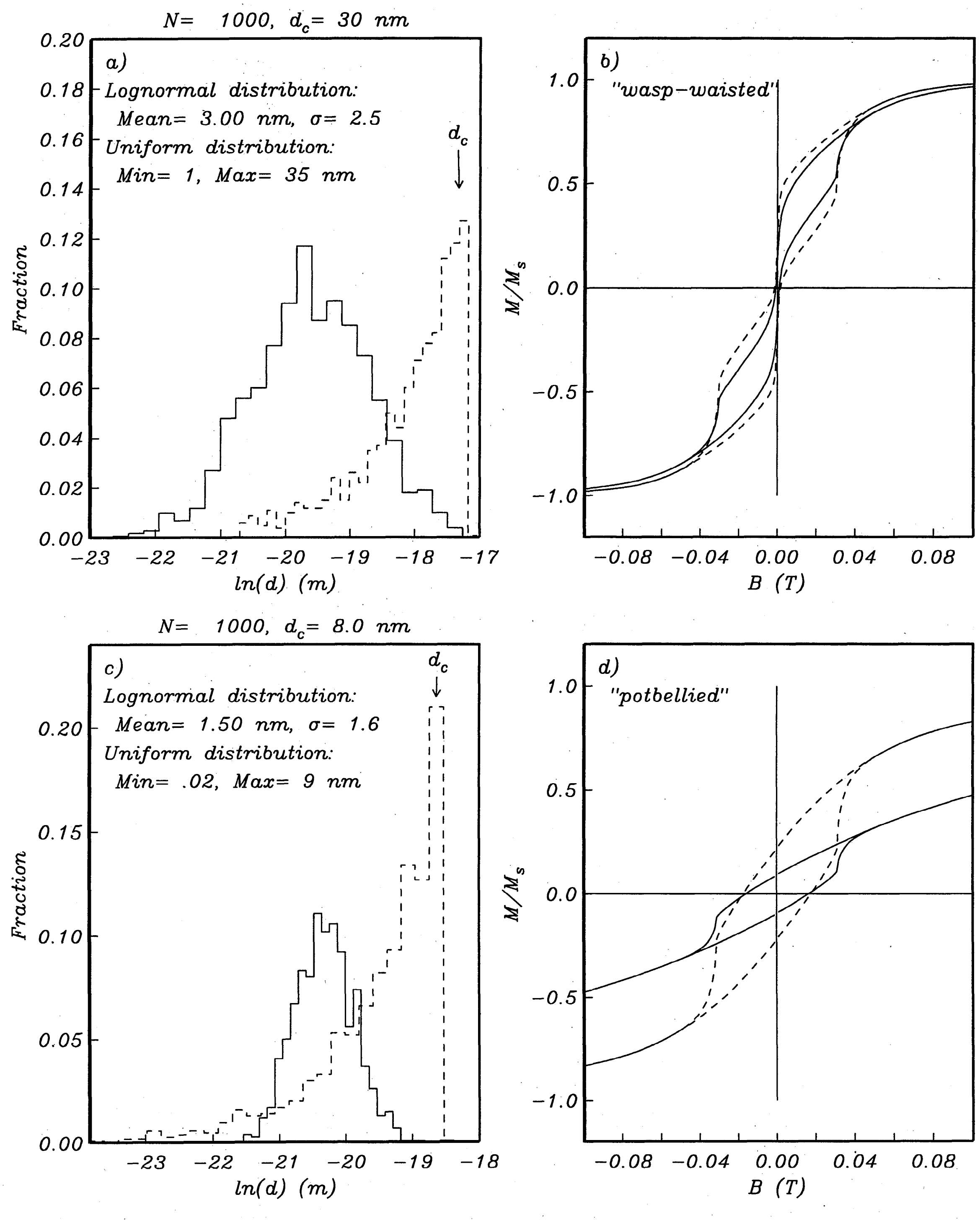

Figure 5. Examples of synthetic hysteresis loops using the methods described in the text. (a) and (b) Results from lognormal (solid lines) and uniform distribution (dashed lines) using an SP/SD threshold size (d_c) of 30 nm are shown. (c) and (d) show results as in Figures 5a and 5b, but with d_c = 8 nm.

The calculation of ascending and descending loops for ϕ other than 0 is more difficult. The contribution of a particular particle to the descending loop is given by $m_{||}$ = cos $(\alpha)M_s v$. We require the value of θ that results in a minimum in E or equivalently results in (11) being 0 and (12) being positive. We do this numerically.

Normalizing by M_s and substituting in d, we get $m_{||}$/m = cos $(\alpha)d^3$. The descending loop is evaluated for values of B from B_{max} to 0. The ascending loop is calculated in two parts. We begin with $m_{||}$ = -cos $(\alpha)M_s d^3$, evaluating $m_{||}$ for $B = 0$ to B_{max} until the flipping field B_f is reached. (The sign of magnetization is negative because this is the remanent magnetization resulting from initial exposure to $-B_{max}$). At this point the ascending curve jumps to the descending curve and is evaluated as before. See Figure 4a (ϕ = 22°and 70°) for examples.

In the case of ϕ = 90°, the "loop" reduces to a line. Starting with $B = +B_{max}$, the moment is entirely "bent" into the field direction, and $m_{||}/m$ = 1. However, when B is less than the intrinsic coercivity, the moment begins to relax back into the easy direction, and θ is zero in zero field. Thus $m_{||}$ is zero. Between 0 and B'_c, $m_{||}/m$ is a linear function of B, as shown in Figure 4a.

We generate a synthetic hysteresis loop as before, drawing 10,000 random values of ϕ and summing the contribution to the loop. B'_c is related to the uniaxial anisotropy in our models by $B'_c = 2K_u/M_s$, where M_s is the saturation moment/unit volume (saturation magnetization). We have taken what at first seems the paradoxical approach of assuming a value for the uniaxial anisotropy equal to the magnetocrystalline anisotropy constant K_1 of magnetite. In fact, the magnetocrystalline anisotropy in magnetite at room temperature is cubic (not uniaxial) and has four easy axes parallel to the body diagonals of the magnetite crystal. We choose this value simply because it is the minimum value possible for magnetite and seems in many cases appropriate for the SBG data we are attempting to explain. Perhaps for unexplained reasons one of the four axes is slightly preferred thus behaving uniaxially with nearly magnetocrystalline anisotropy values.

Setting K_u to the magnetocrystalline anisotropy and M_s = 4.5 x 10^5 A/m, we calculate an intrinsic coercivity of about 62 mT. Summing the contributions of 10,000 particles with uniform d and B'_c, and with easy axes uniformly distributed on a hemisphere, we get the curve shown in Figure 4b. The so-called "saturation remanence" (M_r) is the y intercept of the descending curve. The theoretical value for uniaxial SD particles is M_r/M_s is 0.5. The bulk coercivity B_c is the x intercept of the ascending loop. Its theoretical value is 0.48 of the intrinsic value, or about 29 mT. These values were duplicated in our numerical simulation. The value of the field necessary to remagnetize half the moments aligned at M_r, thus reducing the net magnetization to 0, is termed the "coercivity of remanence" and is theoretically 1.09 B_c. For cubic anisotropy the appropriate values for ϕ are not uniformly distributed on a hemisphere but can be no more than 55° away from the applied field. Thus the value for M_r/M_s is much higher, having a theoretical value of 0.87.

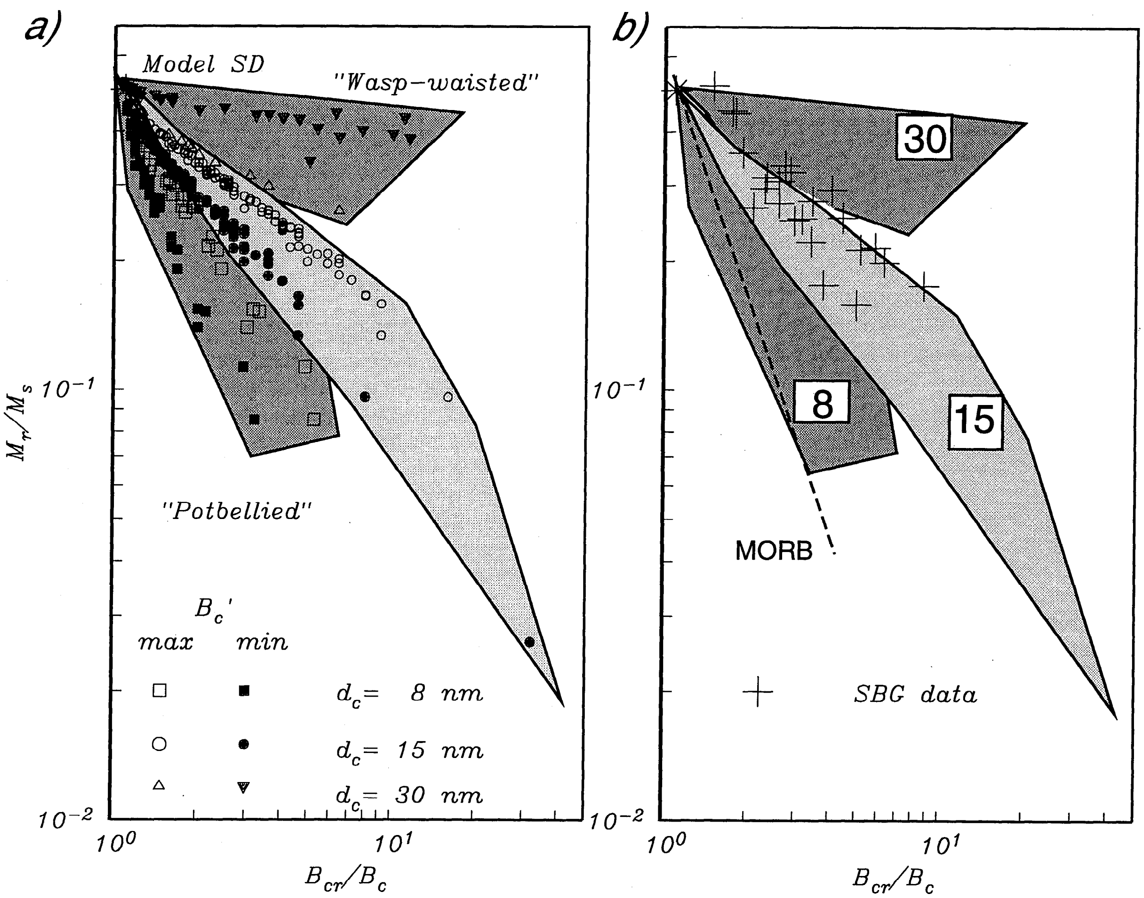

Figure 6. Plots of M_r/M_s on B_{cr}/B_c from simulations using lognormal distributions. (a) Simulations assumming d_c = 30 nm are shown as triangles, those with d_c = 15 nm are circles, and those with d_c = 8 nm are shown as squares. We used the theoretical minimum value of B'_c = 62 mT ($B_o$min) and a value twice that ($B_o$max). The results for $B_o$max are shown as open symbols and those for the minimum are solid. Regions for each d_c are stippled on the diagram. (b) The stippled areas from Figure 6a are shown again and labeled with the assumed threshold size (in nanometers). Results from SBG data are plotted as plus signs. The power law trend for MORB from *Gee and Kent* [1995] shown as a dashed line.

The reversible portions of the single-domain hysteresis loop are drawn as solid lines in Figure 4b. Along these lines, application and removal of a field results in the magnetization traveling along the line. The portions of the loop with irreversible behavior are shown as dashed lines. In these regions, removal of the field results in the magnetization traveling along a different trajectory. For example, application of $-B_{cr}$ results in the magnetization traveling along the trajectory toward zero. The descending and ascending loops therefore have different shapes, and the difference between the two is not simply one of cumulative remanence as suggested by *Jackson et al.* [1990].

We plot the difference between the ascending and descending loops for $B > 0$ of Figure 4b in Figure 4c. This curve we term the "ΔM curve". The difference between the two reversible parts of the loop is plotted as a solid line. Note that despite the fact that the behavior is entirely reversible, the ΔM curve decays slowly. The irreversible portion of the ascending loop (dashed in Figure 4b) is quite steep and the difference between this and the ascending curve (dashed in Figure 4c) decays rapidly to zero, when the descending and ascending loops join and the behavior is again reversible.

The derivative of the ΔM curve (here called $d\Delta M/dB$) is shown in Figure 4d. The wiggles in the region 0-20 mT and 40-100 mT result from "noise". In our numerical simulations, the "noise" stems from the fact that we have used a finite number of "particles" (10,000); noise in real data is mostly instrumental. The large hump centered on approximately B_{cr} ($\sim$ 30 mT) reflects the single coercivity of the population. The rise from about 22 mT to the peak (solid line) results from purely reversible behavior, as this is lower than the smallest flipping field of approximately 31 mT (for $\phi = 45°$).

Simulations of Populations of Mixed SP/SD Particles

We are now in a position to calculate synthetic hysteresis loops, if we define a distribution of grain sizes and the limit of SP behavior (the SP/SD threshold size or d_c). We first consider the case thought to be most reasonable for crystallization during quenching of a glass: lognormal distributions. We generate a simulated sample of particle sizes by drawing from a lognormal distribution of given mean $\bar{d}$ and standard deviation σ (using the function GASDEV of *Press et al.* [1986]). Choosing a value for d_c, we calculate the contribution of the fraction of the sample at each particle size, by first determining if it is SP or SD and then evaluating the volume contribution (scaling by d^3) using the methods outlined in the previous section. Two examples are shown as solid lines in Figure 5 for d_c = 30 nm (Figures 5a and 5b) and 8 nm (Figures 5c and 5d).

As a means of demonstrating that wasp-waisting and potbellying do not depend on having a lognormal distribution, we also considered an unrealistic opposite extreme: a uniform distribution. Uniform distributions were simulated using the RAN1 function of *Press et al.* [1986]. Results from two examples are shown as dashed lines in Figure 5.

It is interesting to note that in hundreds of simulations with different samples of lognormal and uniform distributions in no case were potbellied loops generated using d_c = 30 nm; they were all either SD-like or wasp-waisted. In contrast, no loops generated using d_c = 8 nm were wasp-waisted; they were all either SD-like or potbellied. This can be understood by remembering the strong dependence of initial slope (controlled by B_{90}) on d. The qualitative model of *Pick and Tauxe* [1994] suggests that steep slopes make wasp waists (see Figure 1). Steep slopes require small B_{90}, which in turn require larger grain sizes (see Figure 2). Potbellies are generated by more gentle slopes, requiring larger B_{90}s hence smaller grain sizes. Because the contribution of each size fraction is scaled by volume (d^3), the loops are dominated by the largest grain sizes. More than a few tenths of a percent SD (with a lognormal distribution) results in loops being indistinguishable from SD ($M_r \sim 0.5$ and $B_c/B_c' \sim 1$). For samples just crossing the threshold size, the SP contribution is dominated by the largest SP grains. Thus the effective SP initial slope is just less than d_c and only wasp waists are seen with large d_c. For small d_c there are no SP slopes steep enough to produce wasp-waisting and only "potbellies" appear.

In order to represent a large number of loops on a single diagram, we plot the hysteresis ratios M_r/M_s on B_{cr}/B_c from hundreds of simulated loops (using different lognormal distributions) in Figure 6a. Also shown are results using d_c = 15 nm.

Data from SBG are shown as plus signs on Figure 6b. These lie on top of the region defined by using d_c = 15 nm. Although the results from d_c = 30 using the larger value of B_c partially overlap the field defined by using a $d_c = 15$, the SBG data fall mostly outside the $d_c = 30$ field, and none of the $d_c = 30$ nm loops were potbellied. In nature there is presumably a narrow SP/SD threshold size range for a more or less homogeneous population of particles, and yet both potbellies and wasp-waisted loops are observed. We are attempting to model the results from SBG, partly because we understand a few things about this material (see *Pick and Tauxe* [1993, 1994] for a detailed description): (1) Curie temperatures, blocking temperatures, and transmission electron microscope (TEM) pictures all suggest that the material is relatively homogeneous and consists of low-titanium magnetite. 2) TEM pictures show that the maximum observed particle size is about 20 nm, yet it carries a stable remanence. (3) Low-temperature isothermal remanent magnetization (IRM) experiments suggest that there is a substantial SP fraction in the studied SBGs. 4) The particles appear to be equant (suggesting that the anisotropy energy is dominated by magnetocrystalline anisotropy). (5) The minimum values of B_c measured are about 30 mT, consistent with this observation. Last, the intercept values of M_r/M_s are $\sim$ 0.5 (see Figure 6b), consistent instead with a uniaxial anisotropy. For the moment we argue that for unknown reasons one of the four possible easy axes is preferred thus giving uniaxial behavior with close to magnetocrystalline values of coercivity.

We return now to the strange observation that both wasp waists and potbellies are observed in nature and remember that apparently 20 nm particles of magnetite contribute to the stable remanence (less than the preferred estimate of SP/SD threshold size of $\sim$ 30 nm according to *Dunlop* [1973]). Simulations using a threshold size of 15 nm are shown in Figure 6a and as a shaded region on Figure 6b. For comparison, we plot the data obtained from SBG glasses as solid symbols. Both potbellied and wasp-waisted loops can be generated using a threshold size of some 15 nm. The particular loop generated depends sensitively on the exact grain size distribution. We suggest that both numerical simulation and TEM observations of SBG support a threshold size for SP/SD behavior of substantially less than 30 nm (most likely less than 20 nm).

A second interesting observation from Figure 6 is that the simulated data using each set of parameters follow a power law dependence of the ratios. This is reminiscent of data from marine limestones [*Jackson*, 1990; *McCabe and Channell*, 1994; *Channell and McCabe*, 1994]. In fact, their "Maiolica Limestone" trend would plot within the cloud of data (simulated using d_c = 15 nm and observed in SBG) shown in Figure 6. The loops from the Maiolica are potbellied (see *Channell and McCabe* [1994], Figure 3b right-hand side for a good example). The loops from Trenton, Onondaga, and Knox carbonates are markedly wasp-waisted. These latter plot along a power law trend with a different y intercept. Jackson (1990) suggested that the y intercept of $\sim$ 0.89 pointed to a cubic anisotropy, while *Jackson et al.* [1993] found hints of pyrrhotite in the elevated M_r/M_s ratios. However, in no case were measured values of M_r/M_s in pyrrhotite higher than 0.5 [*Dekkers* 1988]; elevated values appear only after "correction" for "magnetite", so we view the case stronger for cubic anisotropy than for contamination by pyrrhotite (particularly in the absence of other conclusive evidence for pyrrhotite).

A third point concerning the data in Figure 6b is that the ratios from SBG behave rather differently than those from mid-ocean ridge basalts (MORB) [see *Gee and Kent*, 1995]. The hysteresis ratios from the latter plot along the power law trend indicated by the dashed line. Their data include many points with M_r/M_s ratios considerably higher than the maximum of 0.5 observed in SBG and have a different slope. Moreover, the magnetic mineralogy of MORB is dominated by titanomagnetite (TM60) as opposed to the low-titanium magnetite observed in SBG. The reasons for the marked differences between MORB and the sister glass are at present under investigation but could result from initial differences relating to differences in cooling rate and oxygen fugacity, or from differences in sea floor alteration of the two types of materials.

The so-called "Day plot" [*Day et al.*, 1977] of ratios of hysteresis parameters shown in Figure 6 is a very crude description of a hysteresis loop. A single point corresponds to an infinite number of different loop shapes. Yet some compact form of loop representation is desirable because typically a loop is composed of hundreds of individual measurements. In order to partially overcome the limitations of hysteresis loops, *Jackson et al.* [1990] drew from the engineering literature [*Josephs et al.*, 1986] and proposed Fourier analysis of hysteresis loops. The principle attractions are (1) a loop can be adequately characterized by far fewer numbers (some 15-30) than the original measurements (hundreds), (2) data can be smoothed by truncating the Fourier terms to some specified degree, and (3) perhaps shapes can be described by the phase and amplitudes of the Fourier terms.

In Figure 7a we show representative "SD" (solid lines), "wasp-waisted" (dashed lines), and "potbellied" (short-dashed lines) simulated hysteresis loops. In Figure 7b we "unfold" the simulated loops as described by *Jackson et al.* [1990] and *Josephs et al.* [1986]. First, all loops are truncated at 99.9% of M_s. The unfolded loop starts at the point when the descending curve intersects the y axis (M_r). From $B = 0 \rightarrow -B_{\max}$, B is mapped linearly to radians $B' = 0 \rightarrow \pi/2$. From $B = -B_{\max} \rightarrow 0$, B is mapped to $B' = \pi/2 \rightarrow \pi$. From $B = 0 \rightarrow +B_{\max}$, we map B to $B' = \pi \rightarrow 3\pi/2$, and finally, for $B = +B_{\max} \rightarrow 0$, B is converted to $B' = 3\pi/2 \rightarrow 2\pi$. This transformation has the definite advantage that a given value of B' gives a unique value of M/M_s. The different shapes also are readily observed, although the source of the terms "potbelly" and "wasp waist" are no longer obvious. The transformed curves from the wasp-waisted loops fall entirely "outside" the SD curve, having a more "square" waveform, whereas the corresponding potbellied loop, maps to a curve that crosses the SD loop and is more "cone-headed".

The ΔM curves (see Figure 4c) for our simulated loops are shown in Figure 7c. For the SD loop, because $M_r/M_s \sim 0.5$, the difference between the positive y intercept (descending) and the negative y intercept (ascending) is about 1 (see solid line in Figure 7c). Because M_r is depressed in the loops with significant SP fractions in them, those ΔM curves start at lower values. How-

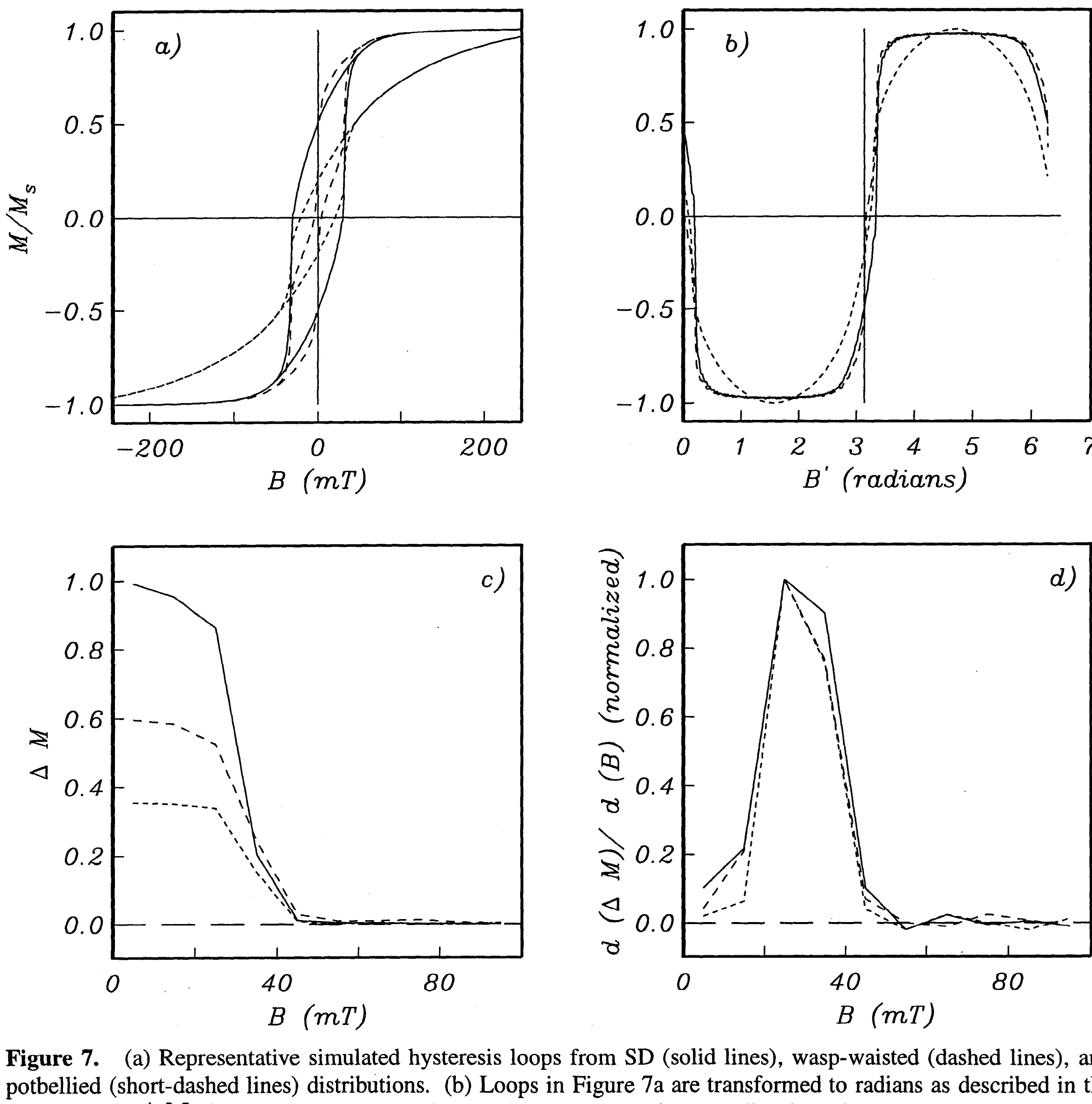

Figure 7. (a) Representative simulated hysteresis loops from SD (solid lines), wasp-waisted (dashed lines), and potbellied (short-dashed lines) distributions. (b) Loops in Figure 7a are transformed to radians as described in the text. (c) The ΔM curves from Figure 7a obtained by subtracting the ascending loop (see caption for Figure 4 for definition) from the descending loop are shown. Curves normalized to unity initial value superpose exactly. (d) The $d\Delta M/dB$ of curves shown in Figure 7c is indicated. One hump means one coercivity fraction in the loop.

ever, because the ΔM curve only reflects the fraction with nonzero y intercepts (the remanent fraction), when normalized to unity, all three superpose. The derivative of the ΔM curve ($d\Delta M/dB$) as shown in Figure 7d should reveal much about the distribution of coercivities contributing to the remanence and as expected, all curves show a single "hump".

Turning now to our experimental data from SBG, consider Figure 8. The data from SBG shown in Figure 1a-c are plotted as ΔM curves in Figures 8a, 8c, and 8e and as $d\Delta M/dB$ in Figures 8b, 8d, and 8f. These data suffer somewhat from instrumental noise and have been moderately smoothed using the Fourier truncation technique (they were truncated to the first 29 terms). The single "hump" in the derivatives is heartening, supporting our claim that the magnetic behavior of SBG is controlled by a single population of particles spanning the SP/SD threshold size [see *Pick and Tauxe*, 1993, 1994].

Two Single-domain Populations With Distinct Coercivity Spectra

The ΔM curve suggests a method whereby some of the different causes of wasp-waisting may be sorted out. *Wasilewski* [1973] showed that wasp-waisted loops could result from mixtures of hematite and magnetite. We have shown that they may also result from mixtures of SP and SD magnetite. How can these be distinguished? In order to address this issue, we first attempted numerical simulation of the problem. In this case we picked randomly oriented grains with coercivities drawn from one of two normal distributions. We vary the means and standard deviations of two lognormal populations of B_c and the fraction of grains drawn from each distribution. One typical result is shown in Figure 9. The ΔM curve shown in Figure 9c does not decrease in a monotonic fashion but behaves more like a "roller coaster". The derivative of the ΔM curve shows two distinct humps reflecting the two coercivity fractions.

In order to investigate what might occur in "real" rocks, we mixed together natural magnetite and hematite. The hematite was taken from the 15-20 μ fraction of sample LH6 separated by *Hartstra* [1982]. The hysteresis loop, ΔM curve, and $d\Delta M/dB$ curves are shown in Figure 10a, 10d, and 10g, respectively. The magnetite was a small piece taken from the sample shown in Figure 1a, and the data are shown in Figure 10b, 10e, and 10h, respectively. Data for the two measured together are shown in Figure 10c, 10f, and 10i, respectively. Again the two humps reflecting the two vastly different coercivities are clearly distinguishable in Figure 10i.

A third mechanism for wasp-waisting was suggested by *Özdemir and Dunlop* [1985]. They observed constricted loops in a single crystal of highly oxidized titanomagnetite. Wasp-waisting in such crystal presumably results from magnetostatic or exchange interactions, a phenomenon we explicitly ignore here.

Summary and Conclusions

1. Distorted hysteresis loops such as the potbellied and wasp-waisted loops obtained from SBG (and other materials) can be mimicked using linear combinations of SP/SD behavior from specified grain size distributions.
2. Wasp waists result from large SP particles and potbellies result from small SP particles. Potbellies are not observed when the SP/SD threshold size is chosen as large as 30 nm. Wasp waists are not observed for thresholds as small as 8 nm.
3. Both potbellied and wasp-waisted loops can be generated using a threshold of about 15-20 nm consistent with TEM/hysteresis observations of SBG.

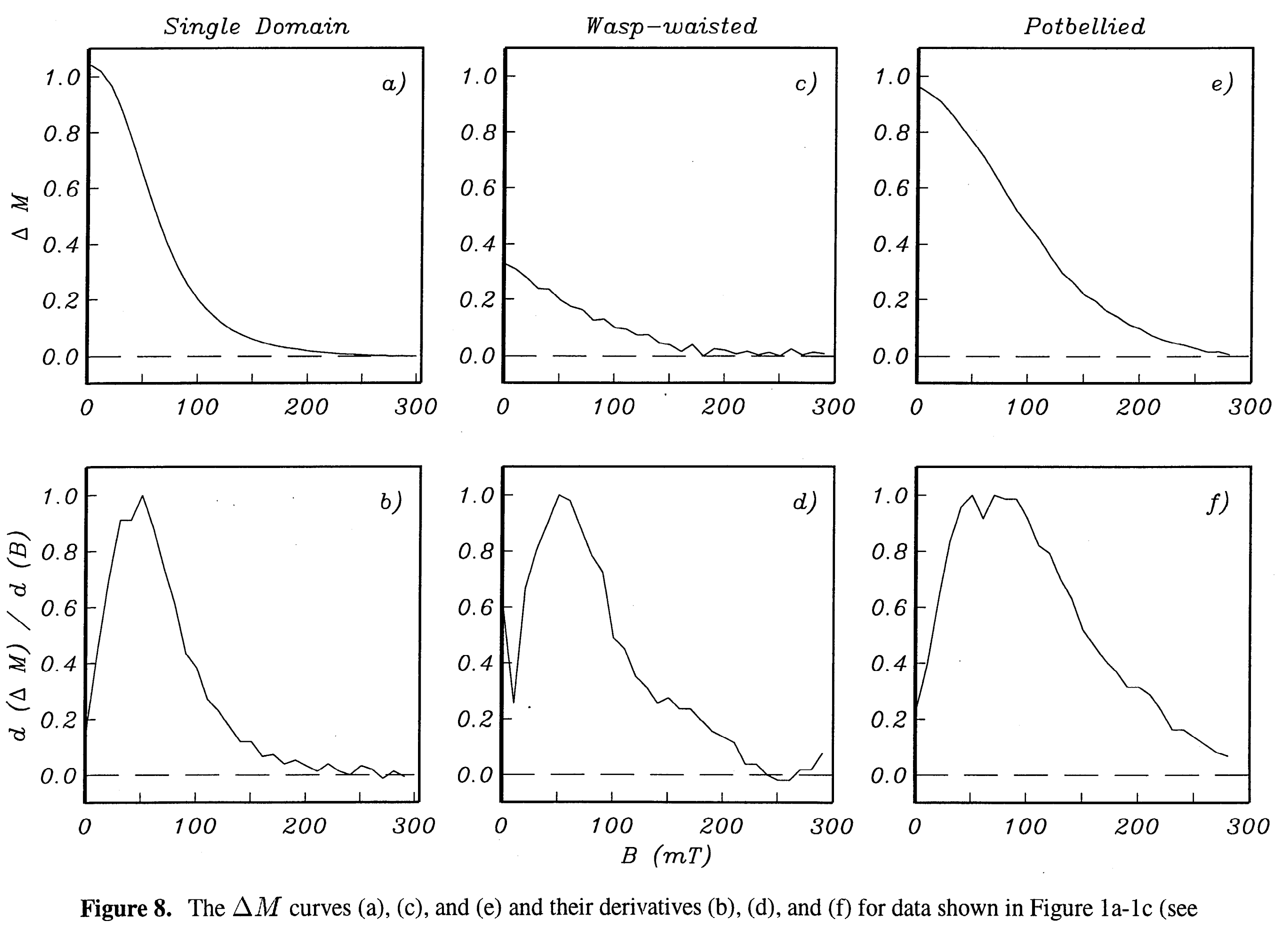

Figure 8. The ΔM curves (a), (c), and (e) and their derivatives (b), (d), and (f) for data shown in Figure 1a-1c (see Figure 7 caption and text).

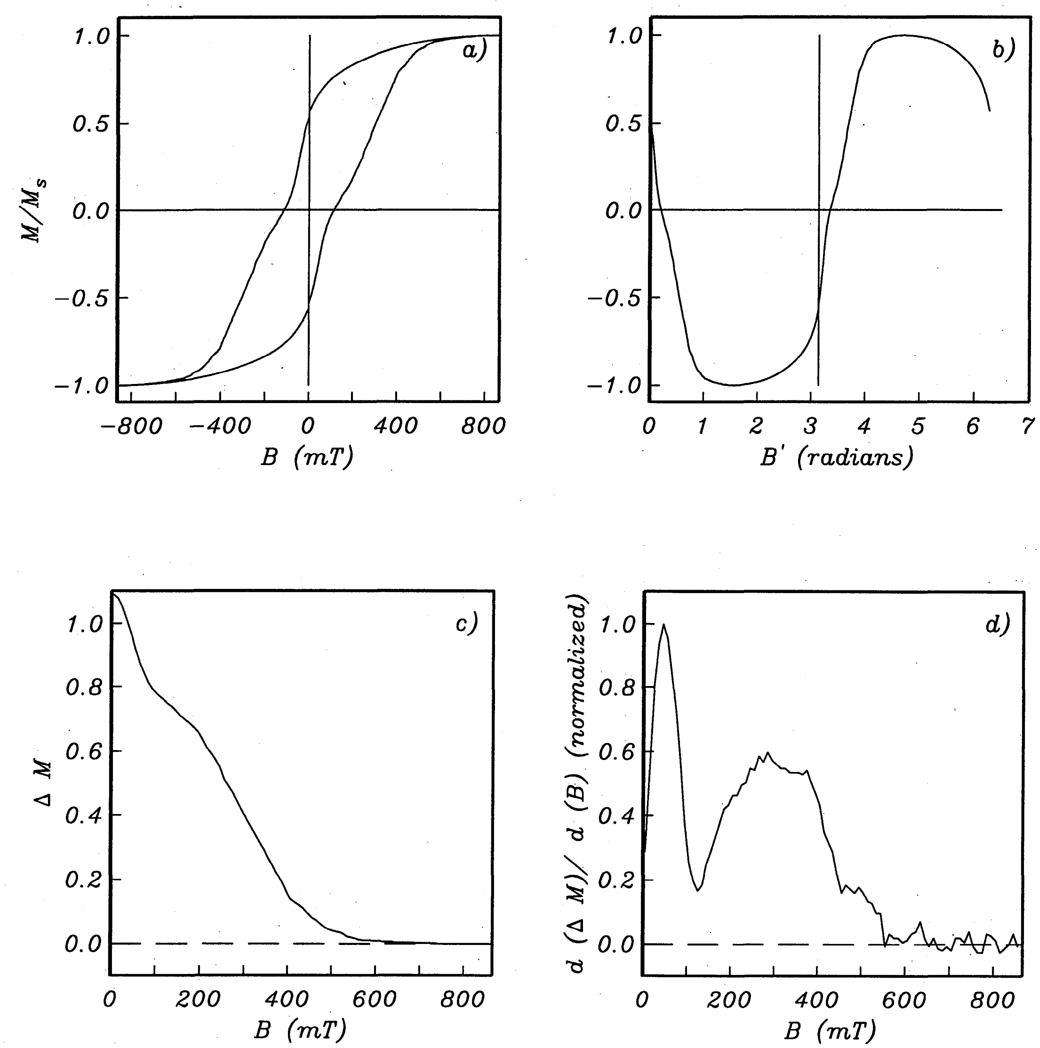

Figure 9. (a) Simulated hysteresis loop for 1000 randomly oriented grains, 25% were drawn from a normal distribution having a mean B_c' of 100 mT and a σ of 50. The rest were drawn from a distribution with mean of 600 mT and σ of 200. (b) The "unfolded loop" from Figure 9a is shown. (c) The ΔM curve (see caption for Figure 7) is shown, and (d) the derivative of Figure 9c is shown.

4. The ΔM curves from all SP/SD simulations and SBG data show a monotonic decrease with increasing field. Saturation (zero difference between ascending and descending loops hence zero cumulative remanence) is achieved in all cases by less than about 200 mT, consistent with IRM acquisition data. These are suggestive of a single SD remanent phase.

5. Wasp-waisting resulting from two populations with distinct coercivities can be distinguished from wasp-waisting resulting from a population spanning the SP/SD threshold by examining the ΔM curves: monotonic decrease can be interpreted as a single population of remanence-carrying particles, whereas "roller coasters" reveal multiple coercivity fractions. The point of zero cumulative remanence is the point at which saturation is achieved.

6. "Power law" trends can result from subtle differences in grain size distributions straddling the SP/SD threshold size. Our simulations look very much like data obtained from certain marine limestones (e.g., the unremagnetized Maiolica and the (white) Scaglia Ammonitica Rosso limestones of *Channell and McCabe* [1994]). Other limestones (e.g., the Paleozoic carbonates of North America) also follow power law trends but with different slopes and may result from two distinct magnetic phases or a different model of anisotropy (e.g., cubic). We believe that numerical simulations using various combinations of magnetic phases as well as allowing cubic anisotropy, when compared with the measured hysteresis loops, can be used to distinguish the various possible causes of the power law trends in the Paleozoic limestones. For example, examination of cumulative curves would conclusively identify multiple coercivity fractions and suggest possible candidates for contamination. We note that where one phase (magnetite) is dominant (the white Scaglia Rossa and the Maiolica), the data behave exactly as our simulations of SP/SD populations in magnetite. The pink Scaglia rossa and the remagnetized Paleozoic limestones fall well above the trend, and simulations using parameters suitable for hematite, goethite, and pyrrhotite could point to one or the other as plausible candidates for contamination.

7. "Day plots" to determine the grain size of the magnetic fraction should be used with extreme caution. Careful examination of the loops for distortions such as potbellying or wasp-waisting is essential as are other tests for the importance of SP grains (for example, measuring of loops at colder temperatures).

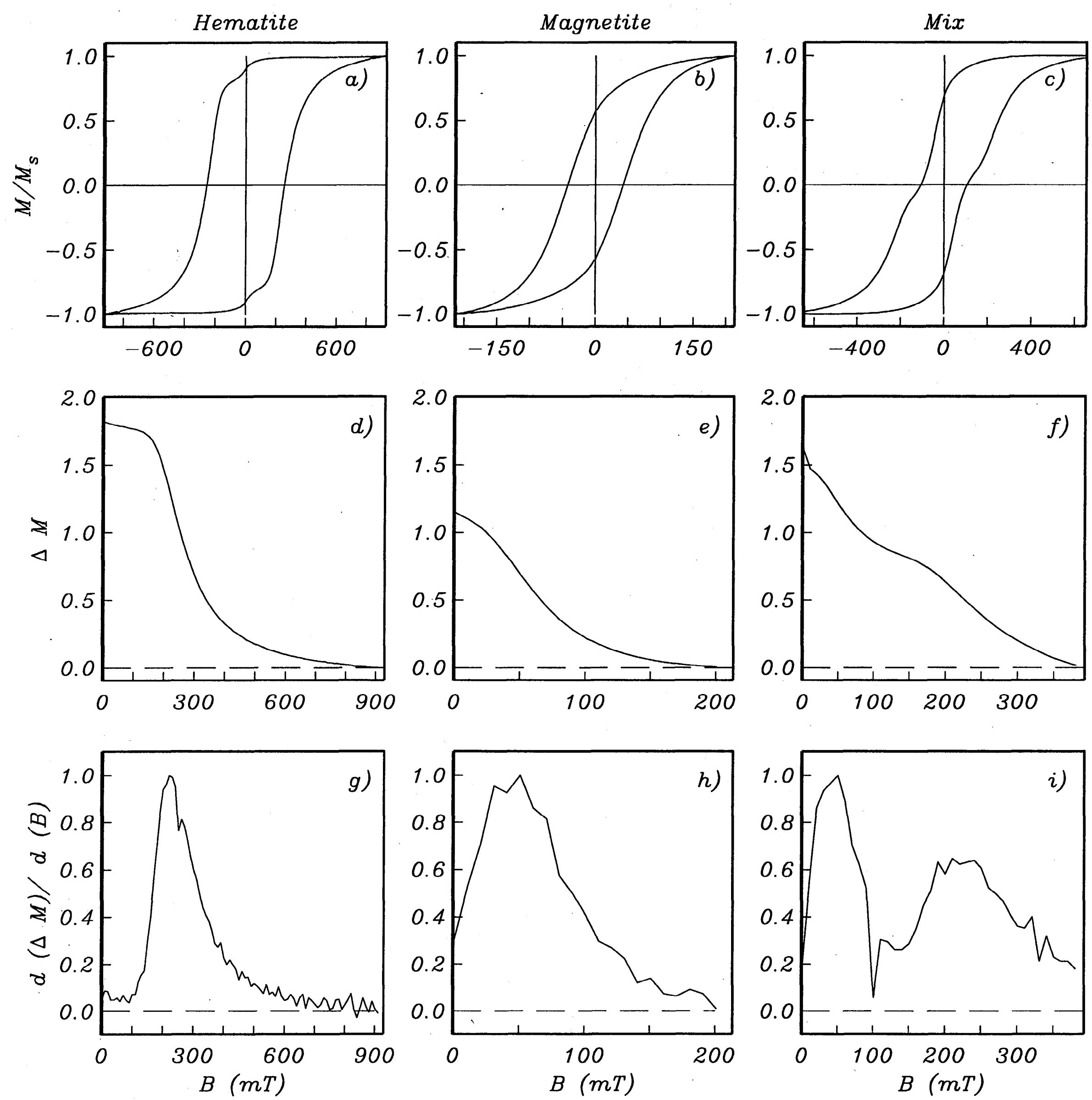

Figure 10. (a), (d), and (g) Data from hematite (LH6 15-20 μ fraction from *Hartstra*, [1982]). (b), (e), and (h) Data from a piece of SBG are shown. (c), (f), and (i) Data obtained from mixing the two are shown. Figures 10a-10c are hysteresis loops; Figures 10d - 10f are ΔM curves and Figures 10g - 10i are derivatives of ΔM curves. Wasp-waisting is observed, but the derivatives of the ΔM curves reveal multiple populations of coercivity thus distinguishing this cause of loop distortion from SP.

Acknowledgments. We are pleased to acknowledge the critical comments of Yvo Kok and S.K. Banerjee. Helpful reviews by B. Moskowitz, Ö. Özdemir, and P. Wasilewski are gratefully acknowledged. We thank C. Constable for comments on the manuscript. This work was partially supported by NSF Grant EAR-9508024 and the Universiteit Utrecht.

References

Argyle, K.S., and D.J. Dunlop, Low-temperature and high-temperature hysteresis of small multidomain magnetites (215-540 nm), *J. Geophys. Res.*, *95*, 7069-7082, 1990.

Basso, V., et al., Experimental study and theoretical interpretation of hysteresis loops and henkel plots in soft magnetic materials, *J. Magn. Magn. Mater.*, *133*, 111-114, 1994.

Borradaile, G.J., N. Chow, and T. Werner, Magnetic hysteresis of limestones: facies control, *Physics Earth Planet. Inter.*, *76*, 241-252, 1993.

Channell, J.E.T., and C. McCabe, Comparison of magnetic hysteresis parameters of unremagnetized and remagnetized limestones, *J. Geophys. Res.*, *99*, 4613-4623, 1994.

Chikazumi, S. and Charap, S.H., *Physics of Magnetism*, Krieger, Melbourne, Fla., 1986.

Day, R., M.D. Fuller, and V.A. Schmidt, Hysteresis properties of titanomagnetites: grain size and composition dependence, *Phys. Earth Planet. Inter.*, *13*, 260-266, 1977.

Dekkers, M.J., Some rock magnetic parameters for natural goethite, pyrrhotite and fine-grained hematite, Ph.D. dissertation, University of Utrecht, Utrecht, Netherlands, 1988.

Dellatorre, E., F. Vajda, and G. Kahler, Modeling magnetic materials with the complete moving hysteresis model, *J. Magn. Magn. Mater.*, *133*, 6-10, 1994.

Dunlop, D.J., Superparamagnetic and SD threshold sizes in magnetite, *J. Geophys. Res.*, *78*, 1780-1793, 1973.

Dunlop, D.J., A method of determining demagnetizing factor from multidomain hysteresis, *J. Geophys. Res.*, *89*, 553-558, 1984.

Dunlop, D.J., Hysteresis properties of magnetite and their dependence on particle size: A test of PSD remanence models, *J. Geophys. Res.*, *91*, 9569-9584, 1986.

Enkin, R., and D.J. Dunlop, A micromagnetic study of pseudo-single-domain remanenc in magnetite, *J. Geophys. Res.*, *92*, 12,726-12,740, 1987.

Enkin, R.J., and W. Williams, Three-dimensional micromagnetic analysis of stability in fine magnetic grains, *J. Geophys. Res.*, *99*, 611-618, 1994.

Fisher, N.I., T. Lewis, and B.J.J. Embleton, *Statistical Analysis of Spherical Data*, Cambridge Univ. Press, New York, 1987.

Flanders, P.J., An alternating gradient force magnetometer, *J. Appl. Phys.*, *63*, 3940-3945, 1988.

Friedman, G., and I.D. Mayergoyz, Stoner-Wohlfarth hysteresis model with stochastic input as a model of viscosity in magnetic materials, *IEEE Trans. Magn.*, *28*, 2262-2264, 1992.

Gee, J., and D.V. Kent, Magnetic hysteresis in young mid-ocean ridge basalts: Dominant cubic anisotropy?, *Geophys. Res. Lett.*, *22*, 551-554, 1995.

Hartstra, R.L., Some rockmagnetic parameters for natural iron-titanium oxides, Ph.D. dissertation, University of Utrecht, Utrecht, Netherlands, 1982.

Heider, F., D.J. Dunlop, and N. Sugiura, Magnetic properties of hydrothermally recrystallized magnetite crystals, *Science*, *236*, 1287-1290, 1987.

Hodych, J.P., Magnetic hysteresis as a function of low temperature in rocks: Evidence for internal stress control of remanence in multidomain and pseudo-single domain magnetite, *Phys. Earth Planet. Inter.*, *64*, 21-36, 1990.

Jackson, M., Diagenetic sources of stable remanence in remagnetized Paleozoic cratonic carbonates: A rock magnetic study, *J. Geophys. Res.*, *95*, 2753-2761, 1990.

Jackson, M., H.-U. Worm, and S.K. Banerjee, Fourier analysis of digital hysteresis data: Rock magnetic applications, *Phys. Earth Planet. Inter.*, *65*, 78-87, 1990.

Jackson, M., P. Rochette, G. Fillion, S.K. Banerjee, and J. Marvin, Rock magnetism of remagnetized Paleozoic carbonates: Low-temperature behavior and susceptibility characteristics, *J. Geophys. Res.*, *98*, 6217-6225, 1993.

Jiles, D.C., Numerical determination of hysteresis parameters for the modeling of magnetic properties using the theory of ferromagnetic hysteresis, *IEEE Trans. Magn.*, *28*, 27-35, 1992.

Josephs, R.M., D.S. Crompton, and C.S. Krafft, Characterization of magnetic oxide recording media using Fourier analysis of static hysteresis loops, *IEEE Trans. Magn.*, *MAG-22*, 653-655, 1986.

McCabe, C., and J.E.T. Channell, Late Paleozoic remagnetization in limestones of the Craven Basin (northern England) and the rock magnetic fingerprint of remagnetized sedimentary carbonates, *J. Geophys. Res.*, *99*, 4603-4612, 1994.

O'Reilly, W., *Rock and Mineral Magnetism*, Blackie, Glasgow, 1984.

Ossart, F., and G. Meunier, Results of modeling magnetic hysteresis using the finite-element method, *J. Appl. Phys.*, *69*, 4835-4837, 1991.

Özdemir, Ö., and D.J. Dunlop, An experimental study of chemical remanent magnetizations of synthetic monodomain titanomaghemites with initial thermoremanent magnetizations, *J. Geophys. Res.*, *90*, 11,513–11,523, 1985.

Parry, L.G., Shape-related factors in the magnetization of immobilized magnetite particles, *Phys. Earth Planet. Inter.*, *22*, 144-154, 1980.

Parry, L.G., Magnetization of immobilized particle dispersions with two distinct particle sizes, *Phys. Earth Planet. Inter.*, *28*, 230-241, 1982.

Pick, T., and L. Tauxe, Holocene paleointensities: Thellier experiments on submarine basaltic glass from the East Pacific Rise, *J. Geophys. Res.*, *98*, 17,949-17,964, 1993.

Pick, T. and L. Tauxe, Characteristics of magnetite in submarine basaltic glass, *Geophys. J. Int.*, *119*, 116-128, 1994.

Press, W.H., B.P. Flannery, S.A. Teukolsky, and W.T. Vetterling, *Numerical Recipes: The Art of Scientific Computing*, Cambridge Univ., Press, New York, 1986.

Roberts, A.P., Y. Cui, and K.L. Verosub, Wasp-waisted hysteresis loops: Mineral magnetic characteristics and discrimination of components in mixed magnetic systems, *J. Geophys. Res.*, *100*, 17,909-17,924, 1995.

Senanayake, W.E., and M.W. McElhinny, Hysteresis and susceptibility characteristics of magnetite and titanomagnetites: Interpretation of results from basaltic rocks, *Phys. Earth Planet. Inter.*, *26*, 47-55, 1981.

Sprowl, D., Numerical estimation of interactive effects in single-domain magnetite, *Geophys. Res. Lett.*, *17*, 2009-2012, 1990.

Stacey, F.D., and S.K. Banerjee, *The Physical Principles of Rock Magnetism*, Elsevier, New York, 1974.

Stoner, E.C., and W.P. Wohlfarth, A mechanism of magnetic hysteresis in heterogeneous alloys, *Philos. Trans. R. Soc. London, A 240*, 599-642, 1948.

Sun, W., and M. Jackson, Scanning electron microscopy and rock magnetic studies of magnetic carriers in remagnetized early Paleozoic carbonates from Missouri, *J. Geophys. Res.*, *99*, 2935-2942, 1994.

Tarduno, J.A., Temporal trends of magnetic dissolution in the pelagic realm: Gauging paleoproductivity?, *Earth Planet. Sci. Lett.*, *123*, 39-48, 1994.

Walker, M., P.I. Mayo, K. O'Grady, S.W. Charles, and R.W. Chantrell, The magnetic properties of single-domain particles with cubic anisotropy, I, Hysteresis loops, *J. Phys. Condens. Matter*, *5*, 2779-2792, 1993a.

Walker, M., P.I. Mayo, K. O'Grady, S.W. Charles, and R.W. Chantrell, The magnetic properties of single-domain particles with cubic anisotropy, II, Remanence curves, *J. Phys. Condens. Matter*, *5*, 2793-2808, 1993b.

Wasilewski, P.J., Magnetic hysteresis in natural materials, *Earth Planet. Sci. Lett.*, *20*, 67-72, 1973.

Williams, W. and Dunlop, D.J., Three-dimensional micromagnetic modelling of ferromagnetic domain structure, *Nature*, *337*, 634-637, 1989.

Williams, W., and D.J. Dunlop, Simulation of magnetic hysteresis in pseudo-single domain grains of magnetite, *J. Geophys. Res.*, *100*, 3859-3872, 1995.

Worm, H.-U., and H. Markert, Magnetic hysteresis properties of fine particle titanomagnetites precipitated in a silicate matrix, *Phys. Earth. Planet. Inter.*, *46*, 84-92, 1987.

T.A.T. Mullender, T. Pick, and L. Tauxe, Institute of Earth Sciences, Fort Hoofddijk Paleomagnetic Laboratory, University of Utrecht, Budapestlaan 17, 3584 CD Utrecht, Netherlands (e-mail: ltauxe@geof.ruu.nl)

(Received March 15, 1995; revised September 25, 1995; accepted September 29, 1995.)